The 9th European Congress on Computational Methods in Applied Sciences and Engineering
ECCOMAS Congress 2024
3–7 June 2024, Lisboa, Portugal

MODELLING SAND RIPPLES IN MINE COUNTERMEASURE SIMULATIONS BY MEANS OF STOCHASTIC OPTIMAL CONTROL

P. Blondeel[1], F. Van Utterbeeck[1] and B. Lauwens[1]

[1] Royal Military Academy, Department of mathematics, Avenue de la Renaissance 30
1000 Brussels Belgium, {philippe.blondeel, filip.vanutterbeeck, ben.lauwens}@mil.be

Key words: Stochastic Optimal Control, Mine Countermeasures, Sand Ripples

Summary. Modelling and simulating mine countermeasures (MCM) search missions performed by autonomous vehicles equipped with a sensor capable of detecting mines at sea is a challenging endeavour. In this work, we present a novel way to model and account for sand ripples present on the bottom of the ocean while calculating trajectories for the autonomous vehicles by means of a stochastic optimal control framework. It is known from the scientific literature that these ripples impact the sea mine detection capabilities of the autonomous vehicles.

1 INTRODUCTION

Modelling and simulating mine countermeasures (MCM) search missions performed by autonomous vehicles is a challenging endeavour. The goal of these simulations typically consists of computing trajectories for the autonomous vehicles in a designated zone such that the residual MCM risk in said zone is below a certain threshold while simultaneously ensuring that the mission time stays below a certain value. This type of problem is referred to as a Coverage Path Planning (CPP) problem, see [1, 2, 3, 4, 5, 6, 7, 8]. From the previously cited works, two main approaches emerge. The first one consists of decomposing the to-be surveyed zone into a grid made from square or hexagonal cells. This grid is then used to compute a trajectory for the autonomous vehicle such that each cell is visited at least once. The second approach consists of computing a trajectory according to a pattern such as, a boustrophedon pattern, a zigzag search pattern or a weaving pattern. However, a novel third approach is presented in the work of [9]. There, the CPP problem is formulated as a stochastic optimal control problem. A major advantage of this approach consists of its extensibility. Meaning that from an implementation standpoint, it is straightforward for the end-user to add additional autonomous vehicles in the to-be surveyed zone. The trajectories for the multiple vehicles are then computed simultaneously resulting in a lower mission time.

From the work of [10], it is known that the characteristics of the ocean floor impact the detection of mines. The presence of sand ripples, which can be viewed as sand dunes on the ocean floor, impact the detection capabilities of the autonomous vehicles when arising in the to-be surveyed zone. In order to be able to detect mines when sand ripples are present, the autonomous vehicles need to traverse the ripples in a perpendicular way.

In this paper, we start from the work of [9], and implement the MCM search mission formulation in a stochastic optimal control framework, see [11], such that the mission time is minimized

while ensuring that the residual MCM risk in the to-be surveyed zone is below a certain threshold. The main contribution of this work consists of the novel formulation and implementation used to account for sand ripples when computing trajectories by means of a stochastic optimal control framework.

The paper is structured as follows. First we present the methodology, where we introduce the sensor model, the formulation of the stochastic optimal control problem, and our modelization of the sand ripples in the stochastic optimal control framework. Second, we present results where we show how the trajectories are adapted when sand ripples are present in the to-be surveyed zone. We present results for up to two autonomous vehicles acting in the same zone.

2 METHODOLOGY

In this section, we first present the equations describing the sensor model for a Forward Looking Sensor (FLS), i.e., a sensor which is only capable of detecting the presence of sea mines when they are located in front of the autonomous vehicle. Hereafter, we give the equations pertaining to the stochastic optimal control problem as set forward in [9]. Last, we present our approach on how to account for sand ripples when using the stochastic optimal control framework.

2.1 Sensor Model

We briefly introduce the equations pertaining to the modelisation of a FLS. A more detailed description can be found in [9].

The sensor model is given by

$$\gamma\left(\boldsymbol{x}\left(t\right),\boldsymbol{\omega}\right) := \lambda\, p\left(\boldsymbol{x}\left(t\right),\boldsymbol{\omega}\right)\, F_{\alpha}\left(\boldsymbol{x}\left(t\right),\boldsymbol{\omega}\right)\, F_{\varepsilon}\left(\boldsymbol{x}\left(t\right),\boldsymbol{\omega}\right), \tag{1}$$

where λ stands for the Poisson scan rate in s^{-1}.

The sensor model of Eq. (1) consists of three parts. The first part consists of $p\left(\boldsymbol{x}\left(t\right),\boldsymbol{\omega}\right)$ and is given by

$$p\left(\boldsymbol{x}\left(t\right),\boldsymbol{\omega}\right) := \Phi\left(\frac{\mathrm{FOM} - 20\log_{10}\left(\left\|\boldsymbol{\omega}-\boldsymbol{x}\left(t\right)\right\| + a\left\|\boldsymbol{\omega}-\boldsymbol{x}\left(t\right)\right\|\right)}{\sigma}\right), \tag{2}$$

where $\Phi\left(\cdot\right)$ stands for the cumulative density function (CDF) of the normal distribution, FOM is a parameter related to the sonar characteristics, a is the attenuation coefficient in dB/km, and $\boldsymbol{x}\left(t\right)$ is given in Eq. (10). We give $\left\|\boldsymbol{\omega}-\boldsymbol{x}\left(t\right)\right\|$ as

$$\left\|\boldsymbol{\omega}-\boldsymbol{x}\left(t\right)\right\| := \sqrt{\left(\omega_x - x\left(t\right)\right)^2} + \sqrt{\left(\omega_y - y\left(t\right)\right)^2}, \tag{3}$$

where $\boldsymbol{\omega}$ is defined as $\boldsymbol{\omega} := \left(\omega_x, \omega_y\right)$, and stands for the position of the possible target, i.e., a sea mine. This second part, $F_{\alpha}\left(\boldsymbol{x}\left(t\right),\boldsymbol{\omega}\right)$, models the detection of the sensor in front of the autonomous vehicle according to its Field Of View (FOV), and is given as

$$F_{\alpha}\left(\boldsymbol{x}\left(t\right),\boldsymbol{\omega}\right) := \frac{1}{1+e^{p_{\alpha}\left(-\frac{\alpha_{\mathrm{FOV}}}{2}-\alpha^{b}\left(\boldsymbol{x}\left(t\right),\boldsymbol{\omega}\right)\right)}} + \frac{1}{e^{p_{\alpha}\left(\alpha^{b}\left(\boldsymbol{x}\left(t\right),\boldsymbol{\omega}\right)-\frac{\alpha_{\mathrm{FOV}}}{2}\right)}} - 1, \tag{4}$$

where p_α is a parameter used to adjust the slope of the sigmoidal curves, and

$$\begin{aligned} \alpha^b\left(\boldsymbol{x}\left(t\right),\boldsymbol{\omega}\right) &:= \arctan 2\left(dx^b\left(\boldsymbol{x}\left(t\right),\boldsymbol{\omega}\right), dy^b\left(\boldsymbol{x}\left(t\right),\boldsymbol{\omega}\right)\right) \\ dx^b\left(\boldsymbol{x}\left(t\right),\boldsymbol{\omega}\right) &:= \left(\omega_x - x(t)\right)\cos(\psi(t)) + \left(\omega_y - y(t)\right)\sin(\psi(t)) \\ dy^b\left(\boldsymbol{x}\left(t\right),\boldsymbol{\omega}\right) &:= -\left(\omega_x - x(t)\right)\sin(\psi(t)) + \left(\omega_y - y(t)\right)\cos(\psi(t)). \end{aligned} \tag{5}$$

In Eq. (4), α_{FOV} is the Field Of View angle of the FLS in degrees. In Eq. (5), $\psi(t)$ represents the angle the autonomous vehicle has with respect to the horizontal axis in degrees, $x(t)$ is the position along the x-axis and $y(t)$ is the position along the y-axis.

The third part, $F_\varepsilon\left(\boldsymbol{x}\left(t\right),\boldsymbol{\omega}\right)$ accounts for the height h in meters above the ocean floor of the sensor attached to the autonomous vehicle, and is given by

$$F_\varepsilon\left(\boldsymbol{x}\left(t\right),\boldsymbol{\omega}\right) := \frac{1}{1+e^{p_\epsilon\left(\varepsilon_{\text{DE}} - \frac{\varepsilon_{\text{FOV}}}{2} - \varepsilon^b(\boldsymbol{x}(t),\boldsymbol{\omega})\right)}} + \frac{1}{e^{p_\epsilon\left(\varepsilon^b(\boldsymbol{x}(t),\boldsymbol{\omega}) - \varepsilon_{\text{DE}} - \frac{\varepsilon_{\text{FOV}}}{2}\right)}} - 1, \tag{6}$$

where p_ε is a parameter used to adjust the slope of the sigmoidal curves, and

$$\varepsilon^b\left(\boldsymbol{x}\left(t\right),\boldsymbol{\omega}\right) := \arctan\left(\frac{-h}{\|\boldsymbol{\omega} - \boldsymbol{x}\left(t\right)\|}\right), \tag{7}$$

where ε_{FOV} and ε_{DE} respectively stand for the vertical FOV, and the downward elevation angle such that the sensor can ensonify the sea floor. For a more thorough description we refer to [9].

2.2 Trajectories

In [9], the optimization problem was formulated such that the residual MCM risk is minimized for a given mission time. The residual MCM risk is defined as the probability that a team of autonomous vehicles fails to detect the mines in a search area by the end of an MCM operation. The residual MCM risk is sometimes also referred to as the probability of non-detection.

In this work, however we formulated the optimization problem such that the mission time T_f needed to survey a designated zone Ω is minimized for a given residual MCM risk,

$$\min T_f, \tag{8}$$

subjected to

$$\mathbb{E}[q\left(T_F\right)] := \int_\Omega \mathrm{e}^{-\int_0^{T_F}\gamma(\boldsymbol{x}(\tau),\boldsymbol{\omega})\,d\,\tau}\phi\left(\boldsymbol{\omega}\right)d\,\boldsymbol{\omega} \leq \text{residual MCM risk} \tag{9}$$

where $\phi(\cdot)$ is the CDF of the distribution against which we integrate. In this case we consider $\phi(\cdot)$ to be the CDF of the Uniform distribution. We note that in our current approach, a Monte Carlo integration scheme is used to compute the expected value of Eq. (9).

The position of the autonomous vehicle is given by

$$\boldsymbol{x}\left(t\right) := f(x(t), y(t), \psi(t), r(t)), \tag{10}$$

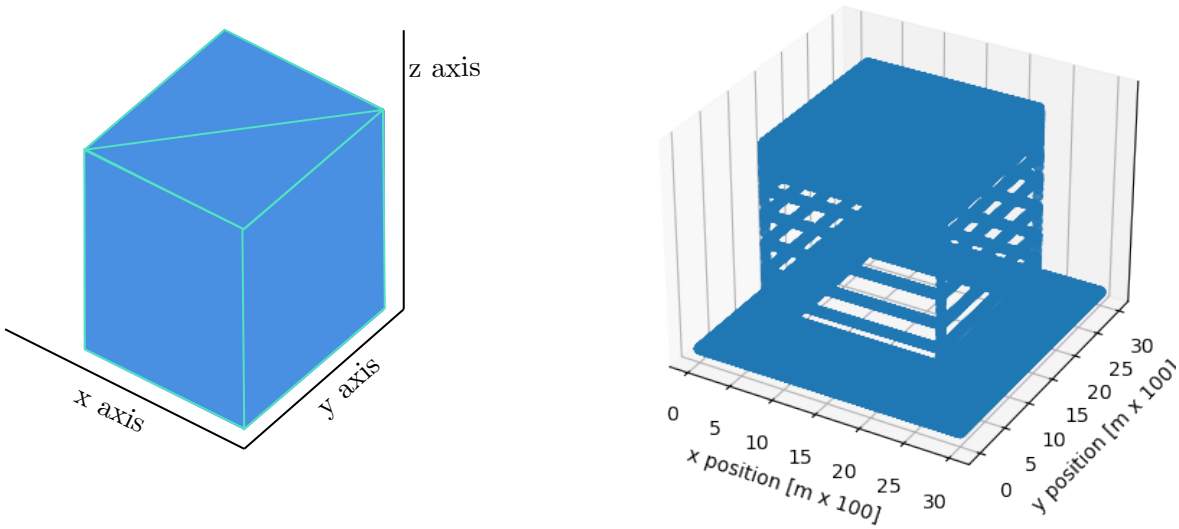

Figure 1: Schematic view the two-dimensional rectangular function (left) and two dimensional rectangular function on the domain $\Omega = [5, 25]^2$ (right).

with $r(t)$ being the turn rate in degrees per second. The position at time t, see Eq. (10), is governed by the following differential equations,

$$\begin{aligned} \frac{d\,x(t)}{d\,t} &= V\cos(\psi(t)) \\ \frac{d\,y(t)}{d\,t} &= V\sin(\psi(t)) \\ \frac{d\,\psi(t)}{d\,t} &= r(t) \\ \frac{d\,r(t)}{d\,t} &= \frac{1}{T}\left(Kp(t) - r(t)\right), \end{aligned} \tag{11}$$

where V stands for the speed in m/s, K is the Nomoto gain constant with units s^{-1}, T is the Nomoto time constant with units s, and $p(t)$ is the rudder deflection angle given in degrees. The optimization software will control the values for the rudder deflection angle in order to compute a trajectory satisfying the target function and the constraints.

2.3 Modeling of Ripples

The presence of sand ripples in the domain is taken into account by multiplying the gamma function, $\gamma\left(\boldsymbol{x}\left(\tau\right), \boldsymbol{\omega}\right)$ of Eq. (9), with a set of functions dividing the rectangular domain Ω into a zone containing ripples and one not containing ripples,

$$\gamma\left(\boldsymbol{x}\left(t\right), \boldsymbol{\omega}\right)_{\text{new}} = \gamma\left(\boldsymbol{x}\left(t\right), \boldsymbol{\omega}\right) \text{Dom}\left(\omega_x, \omega_y, \psi(t)\right). \tag{12}$$

The domain function, $\text{Dom}\left(x, y, \theta\right)$, is a combination of the soft rectangular function taken from [12], see Fig. 1, and the ripple function see Fig. 2. The ripple function presented here,

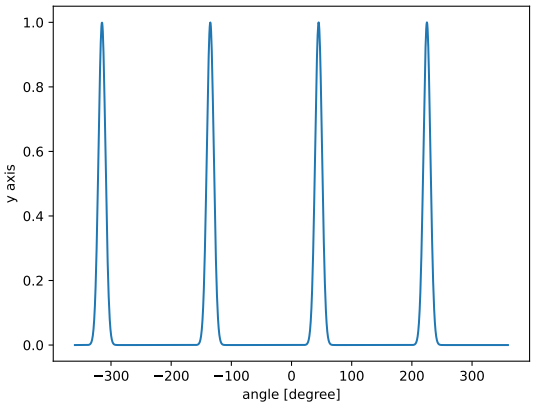

Figure 2: The ripple function for ripples at 135°.

models the sand ripples under an angle of 135°. We have chosen that the soft rectangular function divides the square domain Ω into two triangular zones; one zone where we model sand ripples and one where we do not model sand ripples. This rectangular function is given as

$$\begin{aligned}\mathrm{Rec}\,(x,y) := \\ &\left[\left(\frac{\tanh\left(30\left(x-5\right)\right)-\tanh\left(30\left(x-25\right)\right)}{2}\right)\left(\frac{\tanh\left(30\left(y-x\right)\right)-\tanh\left(30\left(y-25\right)\right)}{2}\right)\right]+ \\ &\left[\left(\frac{\tanh\left(30\left(x-5\right)\right)-\tanh\left(30\left(x-25\right)\right)}{2}\right)\left(\frac{\tanh\left(30\left(y-25\right)\right)-\tanh\left(30\left(y-x\right)\right)}{2}\right)\right].\end{aligned} \tag{13}$$

The ripple function is given as

$$\mathrm{Ripple}\,(\theta) := \sum_{k=-1}^{2} \exp\left(-\frac{\left(\frac{\theta-\pi/4+\pi k}{0.1}\right)^2}{2}\right). \tag{14}$$

The $\mathrm{Dom}\,(x,y,\theta)$ function is given as

$$\begin{aligned}\mathrm{Dom}\,(x,y,\theta) := \\ &\left[\mathrm{Ripple}\,(\theta)\left(\frac{\tanh\left(30\left(x-5\right)\right)-\tanh\left(30\left(x-25\right)\right)}{2}\right)\right. \\ &\left.\left(\frac{\tanh\left(30\left(y-x\right)\right)-\tanh\left(30\left(y-25\right)\right)}{2}\right)\right]+ \\ &\left[\left(\frac{\tanh\left(30\left(x-5\right)\right)-\tanh\left(30\left(x-25\right)\right)}{2}\right)\right. \\ &\left.\left(\frac{\tanh\left(30\left(y-25\right)\right)-\tanh\left(30\left(y-x\right)\right)}{2}\right)\right].\end{aligned} \tag{15}$$

The approach as described here will force the optimization software to select trajectories that are perpendicular to the position of the sand ripples. This is because a contribution to the expected value defined in Eq. (9) will only be made when the autonomous vehicle is travelling in a perpendicular way to the sand ripples.

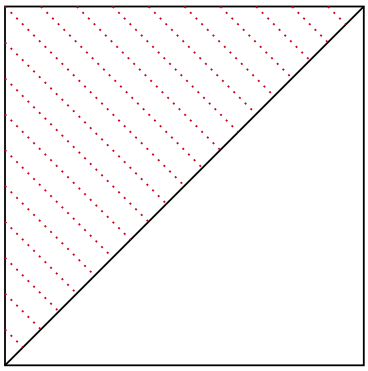

Figure 3: Delimitation of the ripple zone. Sand ripples are present in the upper-left triangle at 135° and depicted by the red dotted line.

3 RESULTS

In this section we present the results when considering one and two autonomous vehicles in a square domain $\Omega = [5, 25]^2$ where sand ripples are present in the upper-left triangle at 135°, see Fig. 3. We consider three different cases. The first case consists of computing the trajectory when no ripples are present in the zone. In the second case, we do not recompute the trajectory, i.e., we use the same trajectory as in case 1, but take into account the presence of sand ripples. This second case mainly serves to illustrate the impact on the residual MCM risk when not taking into account the presence of sand ripples when these are present. The third case shows an updated trajectory which accounts for the presence of the ripples. A brief description of the cases is also given in Tab. 2. For Case 1 and case 3, we requested a residual MCM risk of 10 %. All simulations have been performed on a 16 core Intel i7-12850HX processor with 32GB RAM. The different parameters for our simulations are shown in Tab. 1.

Parameter name	Value
α_{FOV}	120.0^{o}
h	$20.0\,m$
σ	$9.0\,[/]$
λ	$20.0\,s^{-1}$
a	$5.2\,dB/km$
ε_{FOV}	5.0^{o}
ε_{DE}	-6.0^{o}
FOM	$72.0\,[/]$
p_α	$25.0\,[/]$
p_ε	$400.0\,[/]$
V	$2.5\,m/s$
T	$0.5\,s$
K	$5.0\,s^{-1}$

Table 1: Parameters for the simulations.

Case number	Description
1	Computation of trajectory with no ripples present
2	Identical trajectory as case 1 but with ripples present
3	Computation of an updated trajectory accounting for the presence of ripples

Table 2: Description of the different cases.

Case	Residual MCM risk	Mission time	Computation time
1	10.00 %	2088.00 seconds	20.67 seconds
2	55.75 %	2088.00 seconds	/
3	10.00 %	2778.85 seconds	93.18 seconds

Table 3: Results when considering one autonomous vehicle.

3.1 One Autonomous Vehicle

We present the results for the different cases when considering only one autonomous vehicle, in Tab. 3 and Fig. 4. In Fig. 4, the red color represents the zone that has been surveyed by the sensor, while the blue zone has not been surveyed. The detection probability of a mine by the sensor in the red zone is 1.0 or 100 % and 0 % in the blue zone. The black line represents the trajectory of the autonomous vehicle. The coordinates of the starting point for the autonomous vehicle for all the cases is $(14.5, 15.0)$. For case 1, the residual MCM risk is 10.00 %. The mission time necessary to achieve this percentage is 2088.00 seconds. For case 2, the residual MCM risk is 55.75 %, i.e., an increase in risk of 45.75 % point. This result shows the impact on the residual MCM risk when not taking the ripples into account when these are present. For case 3, the residual MCM risk is again 10.00 % but with a longer mission time, i.e., 2778.85 seconds instead of 2088.00 seconds when compared to case 1. Accounting for sand ripples thus increases the mission duration time. The total computation time needed to calculate the trajectory also increases when accounting for sand ripples, from 20.67 seconds to 93.18 seconds.

3.2 Two Autonomous Vehicles

We now present the results for the different cases when considering two autonomous vehicles, in Tab. 4 and Fig. 5. In Fig. 5, the red color represents the zone that has been surveyed by the combined sensors, while the blue zone has not been surveyed. The detection probability of a mine by the combined sensors in the red zone is 1.0 or 100 % and 0 % in the blue zone. The black lines represent the trajectories of the autonomous vehicles. The conclusions are similar to the ones made when considering only one autonomous vehicle. For case 1, the residual MCM risk is 10.00 %. The mission time necessary to achieve this percentage is 1303.88 seconds. For case 2, the residual MCM risk is 57.18 %, i.e., an increase in risk of 47.18 % point. For case 3, the residual MCM risk is again 10.00 % but with a longer mission time, i.e., 1548.00 seconds instead of 1303.88 seconds when compared to case 1. The mission duration time again increases when considering sand ripples. The total computation time also increases, from 64.22 seconds for case 1 to 118.25 seconds for case 3.

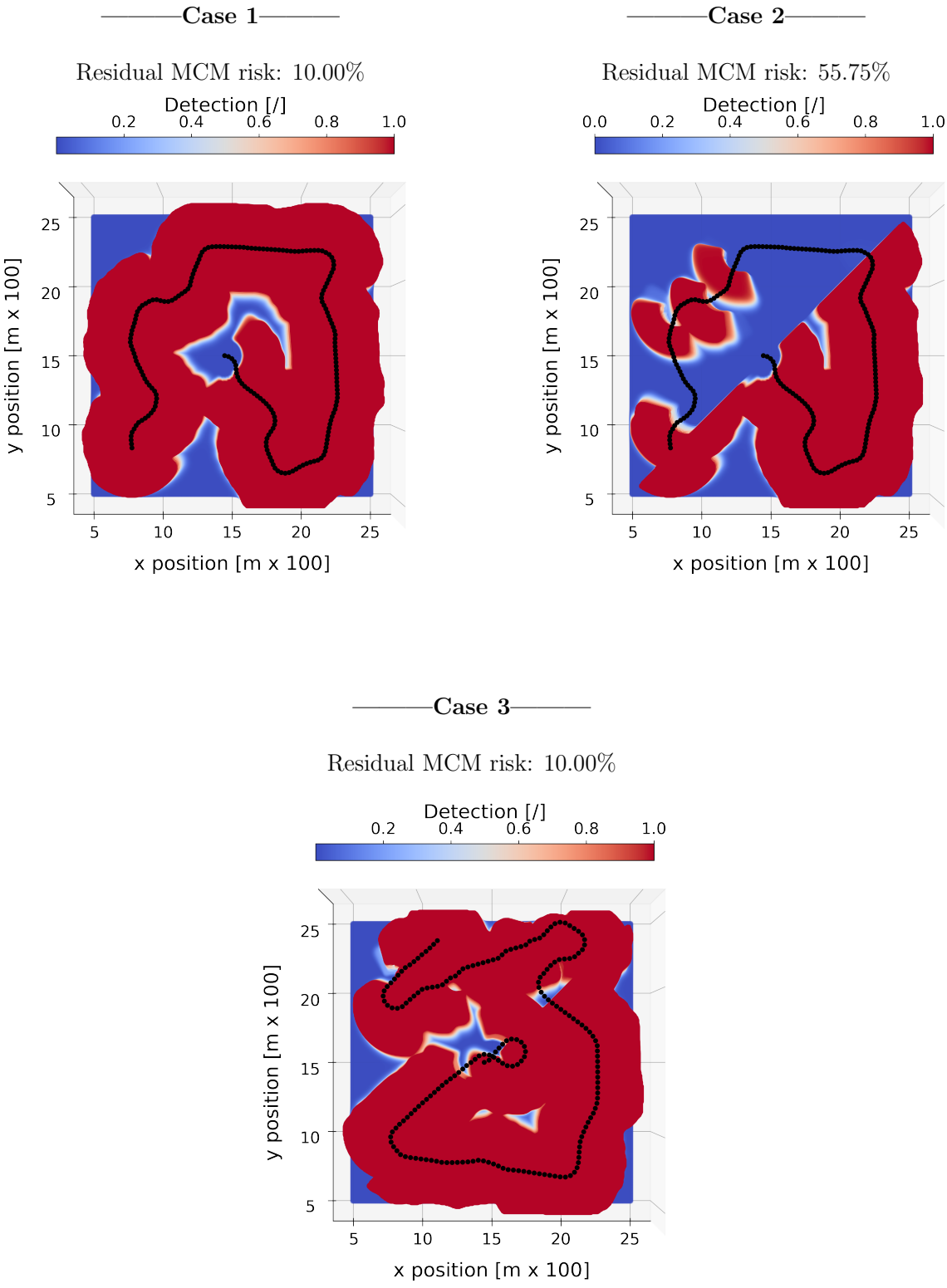

Figure 4: Trajectories and residual MCM risks, see Tab. 3, for the results of the different cases as defined in Tab. 2. The red color represents the zone that has been surveyed by the sensor, while the blue zone has not been surveyed. The detection probability of a mine by the sensor in the red zone is 1.0 or 100 % and 0 % in the blue zone. The black line represents the trajectory of the autonomous vehicle.

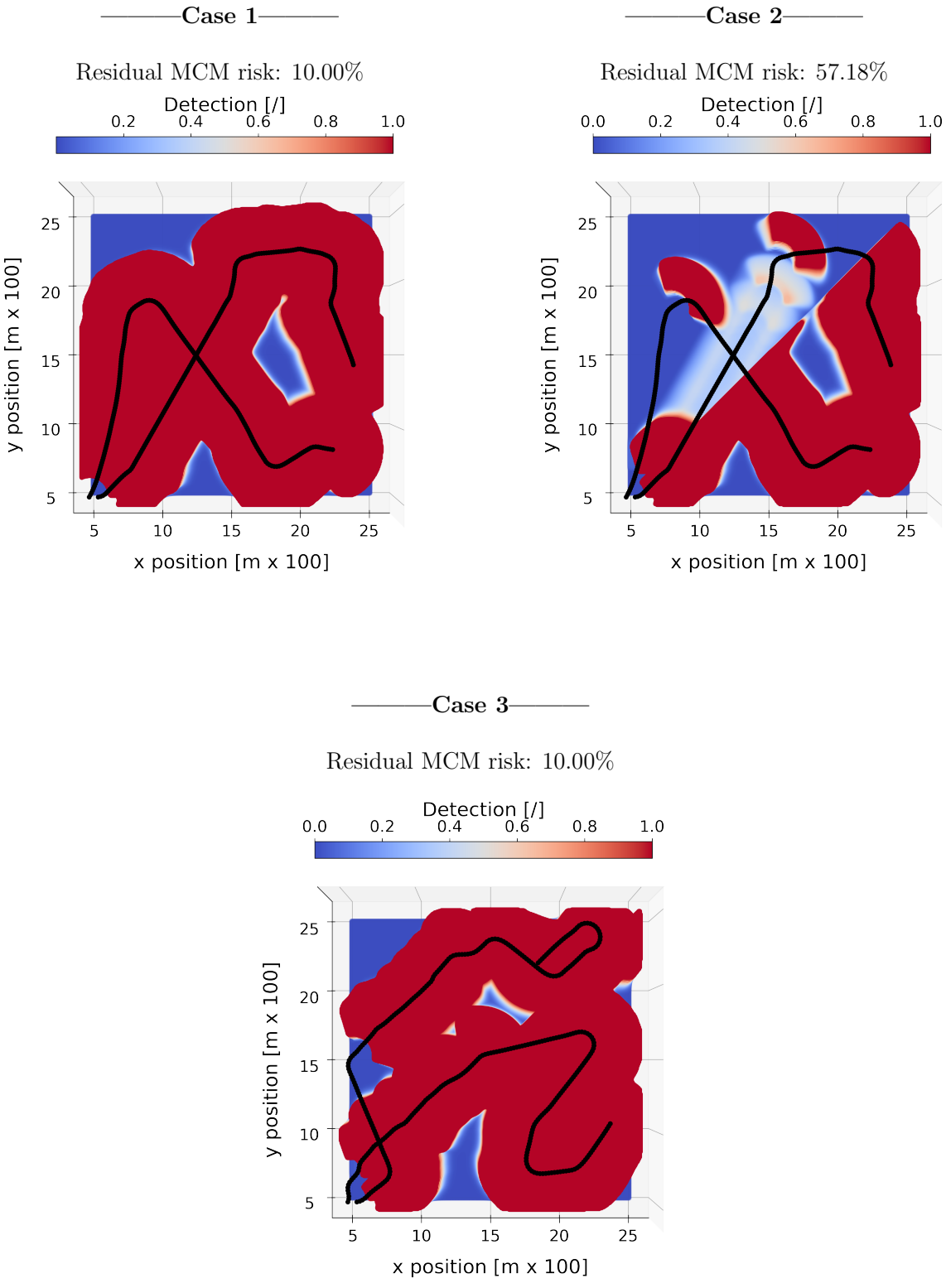

Figure 5: Trajectories and residual MCM risks, see Tab. 4, for the results of the different cases as defined in Tab. 2. The red color represents the zone that has been surveyed by the combined sensors, while the blue zone has not been surveyed. The detection probability of a mine by the combined sensors in the red zone is 1.0 or 100 % and 0 % in the blue zone. The black lines represent the trajectories of the autonomous vehicles.

Case	Residual MCM risk	Mission time	Computation time
1	10.00 %	1303.88 sec	64.22 sec
2	57.18 %	1303.88 sec	/
3	10.00 %	1548.00 sec	118.25 sec

Table 4: Results when considering two autonomous vehicles.

4 CONCLUSION

In this work we presented a novel way to account for sand ripples when computing trajectories for autonomous vehicles by means of a stochastic optimal control approach for mine countermeasure operations in a two-dimensional space. In order to model the presence of sand ripples in a given domain, we constructed a function based on the two-dimensional rectangular function, which we multiplied with the function describing the sensor model. This approach forces the optimization software to compute trajectories for autonomous vehicles that are perpendicular to the sand ripples in the zone where ripples are present. We implemented this for up to two autonomous vehicles in a two dimensional domain $\Omega = [5, 25]^2$, and presented results showing the trajectories for a residual MCM risk of 10 % when considering sand ripples in the domain. We found that the mission time and computational time are larger when simulating the presence of sand ripples. Future work will focus on investigating how to compute trajectories in a non-square domain. Additionally, we plan to investigate if a quasi-Monte Carlo integration scheme for computing the expected value of the residual MCM risk integral can yield a speed-up.

5 REFERENCES

[1] B. Ai, M. Jia, H. Xu, J. Xu, Z. Wen, B. Li, and D. Zhang, "Coverage path planning for maritime search and rescue using reinforcement learning," *Ocean Engineering*, vol. 241, p. 110098, 2021.

[2] H. Choset, "Coverage of known spaces: The boustrophedon cellular decomposition," *Autonomous Robots*, vol. 9, pp. 247–253, 2000.

[3] N. Abreu and A. Matos, "Minehunting mission planning for autonomous underwater systems using evolutionary algorithms," *Unmanned Systems*, vol. 02, no. 04, pp. 323–349, 2014.

[4] M. S. Wiig, T. R. Krogstad, and Ø. Midtgaard, "Autonomous identification planning for mine countermeasures," in *2012 IEEE/OES Autonomous Underwater Vehicles (AUV)*, pp. 1–8, 2012.

[5] E. Galceran and M. Carreras, "A survey on coverage path planning for robotics," *Robotics and Autonomous Systems*, vol. 61, no. 12, pp. 1258–1276, 2013.

[6] C. Cai, J. Chen, Q. Yan, F. Liu, and R. Zhou, "A prior information-based coverage path planner for underwater search and rescue using autonomous underwater vehicle (auv) with side-scan sonar," *IET Radar, Sonar & Navigation*, vol. 16, no. 7, pp. 1225–1239, 2022.

[7] B. Nguyen and D. Hopkin, "Modeling autonomous underwater vehicle (auv) operations in mine hunting," in *Europe Oceans 2005*, vol. 1, pp. 533–538 Vol. 1, 2005.

[8] V. Yordanova and B. Gips, "Coverage path planning with track spacing adaptation for autonomous underwater vehicles," *IEEE Robotics and Automation Letters*, vol. 5, no. 3, pp. 4774–4780, 2020.

[9] S. Kragelund, C. Walton, I. Kaminer, and V. Dobrokhodov, "Generalized optimal control for autonomous mine countermeasures missions," *IEEE Journal of Oceanic Engineering*, vol. 46, no. 2, pp. 466–496, 2021.

[10] V. Yordanova, B. Gips, T. Furfaro, and S. Dugelay, "Coverage path planning for mine countermeasures: Adapting track orientation," in *OCEANS 2019 - Marseille*, pp. 1–7, 2019.

[11] J. L. Pulsipher, W. Zhang, T. J. Hongisto, and V. M. Zavala, "A unifying modeling abstraction for infinite-dimensional optimization," *Computers & Chemical Engineering*, vol. 156, 2022.

[12] I. Schaefer, H. Tal-Ezer, and R. Kosloff, "Semi-global approach for propagation of the time-dependent schrödinger equation for time-dependent and nonlinear problems," *Journal of Computational Physics*, vol. 343, pp. 368–413, 2017.